

Strongly reducing magnesium(0) complexes

<https://doi.org/10.1038/s41586-021-03401-w>

B. Rösch¹, T. X. Gentner¹, J. Eysel¹, J. Langer¹, H. Elsen¹ & S. Harder¹✉

Received: 4 December 2020

Accepted: 26 February 2021

Published online: 28 April 2021

 Check for updates

A complex of a metal in its zero oxidation state can be considered a stabilized, but highly reactive, form of a single metal atom. Such complexes are common for the more noble transition metals. Although rare examples are known for electronegative late-main-group *p*-block metals or semimetals^{1–6}, it is a challenge to isolate early-main-group *s*-block metals in their zero oxidation state^{7–11}. This is directly related to their very low electronegativity and strong tendency to oxidize. Here we present examples of zero-oxidation-state magnesium (that is, magnesium(0)) complexes that are stabilized by superbulky, monoanionic, β -diketiminato ligands. Whereas the reactivity of an organomagnesium compound is typically defined by the nucleophilicity of its organic groups and the electrophilicity of Mg^{2+} cations, the Mg^0 complexes reported here feature electron-rich Mg centres that are nucleophilic and strongly reducing. The latter property is exemplified by the ability to reduce Na^+ to Na^0 . We also present a complex with a linear Mg_3 core that formally could be described as a $\text{Mg}^1\text{–Mg}^0\text{–Mg}^1$ unit. Such multinuclear mixed-valence Mg_n clusters are discussed as fleeting intermediates during the early stages of Grignard reagent formation. Their remarkably strong reducing power implies a rich reactivity and application as specialized reducing agents.

Unique complexes of main group metals and semimetals in the zero oxidation state have been realized as multiply bonded dinuclear entities stabilized by N-heterocyclic carbene (NHC) ligands^{1–4} (Fig. 1a). With π -acidic cyclic alkyl-amino-carbene (CAAC) ligands (Fig. 1b), which are (like CO ligands) strong σ -donors and π -acceptors, mononuclear Si^0 or Ge^0 complexes have been realized^{5,6}. For these complexes, π -backdonation to the CAAC ligands is crucial and serves to reduce the high electron density on the metal(0) centres.

Apart from identification of labile fleeting species^{7–9}, rare early-main-group metal(0) complexes that are stable at room temperature involve the encapsulation of the most electronegative and exotic *s*-block metal, beryllium: $\text{Be}^0(\text{CAAC})_2$ (Fig. 1b)¹⁰. As predicted by theory¹¹, the Be–CAAC bond is a synergistic donor–acceptor bond of considerable covalency. The same computational study predicted that an analogous complex of the more electropositive metal Mg is unstable¹¹. Magnesium, which strongly prefers the oxidation state +II, has been isolated in the form of bimetallic Mg^I complexes^{12,13} (Fig. 1c), but complexation of Mg^0 has hitherto remained elusive¹⁴. Here we report the serendipitous isolation of the first Mg^0 complexes.

Earlier attempts to isolate a mononuclear Mg^I complex with the superbulky β -diketiminato ligand BDI ($\text{HC}\{\text{C}(\text{Me})\text{N}[2,6\text{-}(3\text{-pentyl})\text{-phenyl}]\}_2$) by reduction of **I** led to binuclear Mg^I complex **II** featuring a strongly elongated Mg–Mg bond (Fig. 1d)¹⁵. It is questionable whether highly reactive open shell (BDI) Mg^I radicals can be isolated. Attempts to trap such a radical with a chelating ligand led to dearomatization of the benzene solvent (**III**, Fig. 1d)¹⁵, a process that most recently was also shown to be induced by photoactivation of the Mg–Mg bond¹⁶. Further attempts to isolate a mononuclear Mg^I radical by reduction of **IV**, featuring the even bulkier ligand BDI* ($\text{HC}\{\text{C}(\text{tBu})\text{N}[2,6\text{-}(3\text{-pentyl})\text{-phenyl}]\}_2$), caused Mg–N bond cleavage and gave an asymmetric Mg^I complex with a strongly polarized Mg–Mg bond (**V**, Fig. 2)¹⁷. We found that the

reducing agent has a crucial influence on the reaction outcome: replacing K for the recently introduced¹⁸ Na/NaCl gave dark red-brown crystals of $\{[(\text{BDI}^*)\text{Mg}^-][\text{Na}^+]\}_2$ (**1**) in 48% yield.

The crystal structure of **1** consists of two (BDI*) Mg^- fragments bridged by two Na^+ cations each capped by an aromatic ring (Fig. 3a). Although X-ray diffraction can only give an indication for the Na (11 electrons) and Mg (12 electrons) positions, the metal assignment in **1** is strongly supported by its geometry, reactivity and density functional theory (DFT) calculations (Supplementary Information). Following rules for determination of the formal oxidation state, **1** should be considered a Mg^0 complex with a closed $3s^2$ subshell in which (BDI*) Mg^- could be regarded as isoelectronic to β -diketiminato Al^I complexes¹⁹. Following the rules for Lewis valence electron dot structures, a formal negative charge is placed on Mg. These are, however, formalisms and not actual charges. A similar bonding motif and electronic situation to that in **1** was observed in the first aluminyl potassium complex (Fig. 1e)²⁰. By analogy, **1** could be described as a magnesyl sodium complex. Compounds with a high electron density on *s*-block metals are rare and hitherto only known in the form of alkaliides, for example, $[\text{Na}^-][\text{Na}^+\text{-cryptand}]$ (ref. 21). BDI ligands can be redox-active and are able to accommodate more than one electron²². However, the geometry of the BDI* ligand and the NMR chemical shifts in **1** compare well to those in Mg^I and Mg^I complexes (Supplementary Table 6), indicating that there is no substantial shift of electron density from Mg^0 to the BDI* ligand.

The Mg...Mg distance of 5.7792(5) Å is too long for a bonding interaction. Two Na atoms bridge the Mg atoms with Mg–Na distances of 3.1216(7) Å and 3.4529(7) Å, an asymmetry that is caused by the additional aryl...Na contact. The shortest Mg...Na bond is close to the sum of Bragg's metal radii for Na and Mg (3.19 Å)²³. The long Mg–N bonds in **1** (average: 2.117 Å) are also indicative of a Mg^0 centre; Mg–N bonds

¹Department of Chemistry and Pharmacy, Friedrich-Alexander University Erlangen-Nürnberg, Erlangen, Germany. ✉e-mail: sjoerd.harder@fau.de

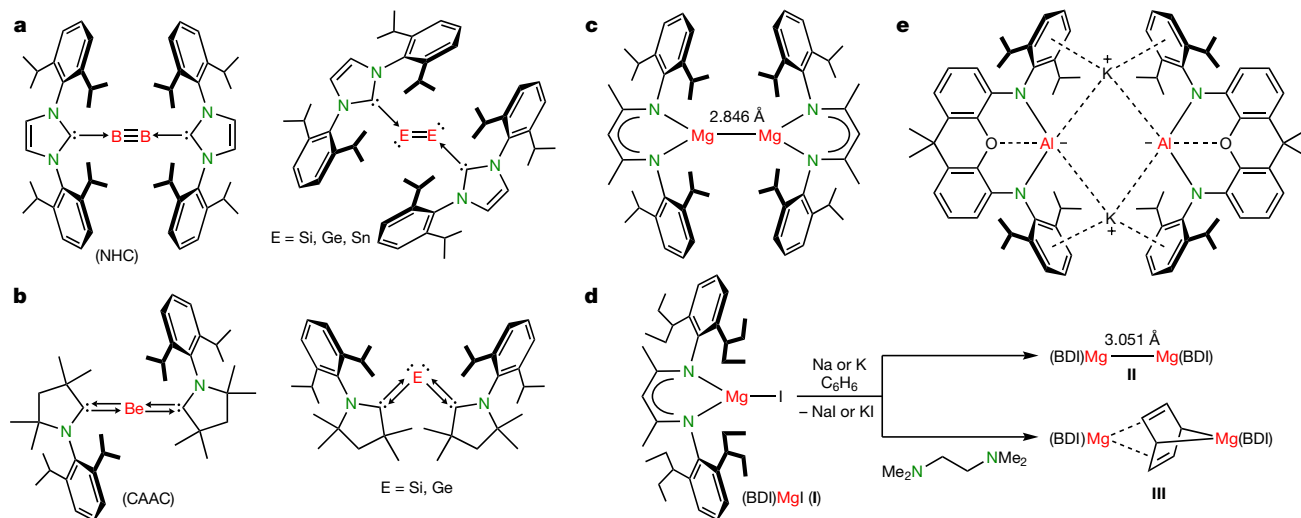


Fig. 1 | Low-valent complexes of main group metals and semimetals.
a, Dinuclear B^0 , Si^0 , Ge^0 and Sn^0 complexes stabilized by NHC ligands.
b, Mononuclear Si^0 , Ge^0 and Be^0 species supported by CAAC ligands.
c, A low-valent dimeric β -diketiminate Mg^I complex. The Mg–Mg bond length

is shown. **d**, Reduction of **I** with Na or K to the binuclear Mg^I complex **II** or **III** (benzene reduction). **e**, A dimeric anionic aluminyl potassium complex. Dashed lines indicate weak coordinative bonds.

shorten with increasing metal oxidation state: compare Mg^I –N (chelating ligand in **V**) 2.064 Å and Mg^{II} –N (**IV**) 1.998 Å.

DFT analysis and charge calculation with natural population analysis (NPA) and atoms-in-molecules (AIM) confirm the electron-rich nature of the Mg^0 centre in **I** (Fig. 3b). The NPA charge of -1.07 on the BDI* ligand is comparable to that on the BDI* ligand in complex **V** (-0.99), corroborating experimental findings that there is no substantial shift of electron density from Mg^0 to the BDI* ligand. The calculated charge on

Mg is $+0.57$ (NPA) or $+0.41$ (AIM); in comparison, the average NPA charge on Mg^I in **II** is $+0.98$ (ref. ¹⁵). Considering that organosodium species are highly ionic²⁴, the rather low charge on Na^+ is remarkable (NPA, $+0.50$; AIM, $+0.74$); in comparison, the charges on Na in complex (BDI*)Na are $+0.91$ (NPA) and $+0.89$ (AIM). This is related to the small difference in Pauling electronegativities between Mg (1.2) and Na (0.9), and implies that some of the Mg^0 electron density is transferred to Na^+ . Complex **I** could therefore also be considered as a $Mg_2Na_2^{2+}$ cluster stabilized by

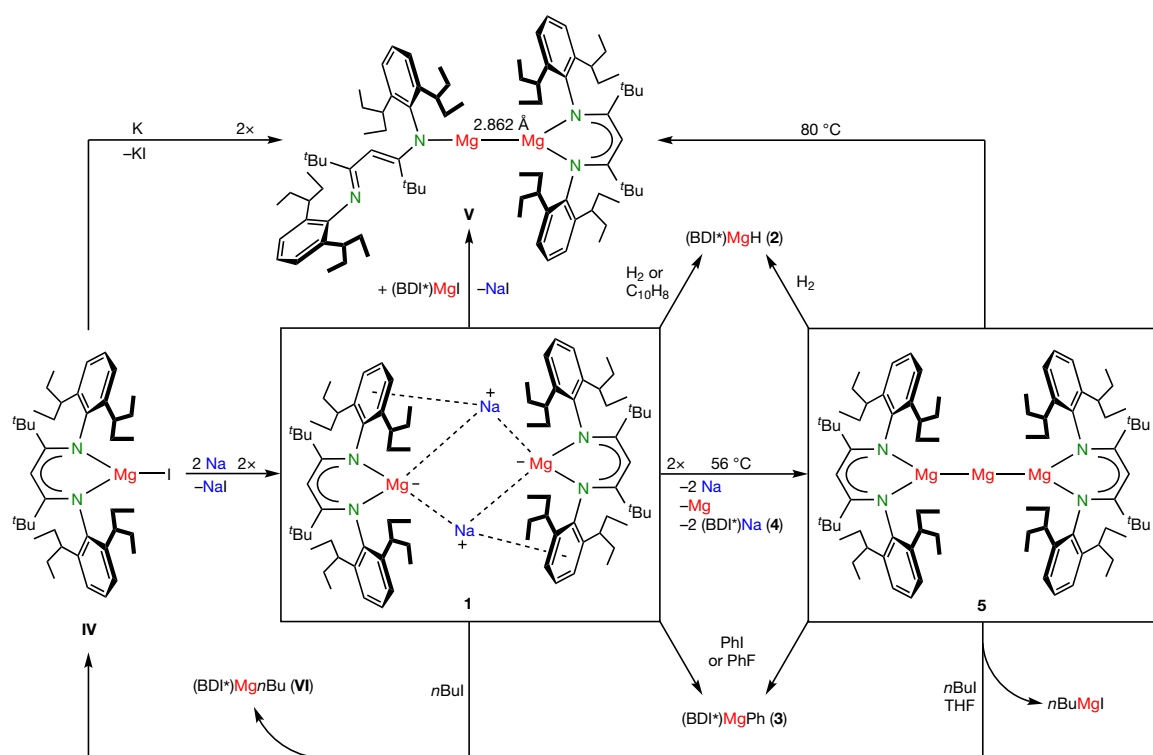


Fig. 2 | Synthesis and reactivity of β -diketiminate Mg^0 complexes. Reduction of **IV** with K gave complex **V**. Employing Na as reducing agent, the $Mg(0)$ complex **I** was isolated. Thermal decomposition of **I** gave **4** and the

mixed-valent Mg complex **5**. Reaction of **1** and **5** with H_2 or arylhalides gave complexes **2** and **3**, respectively.

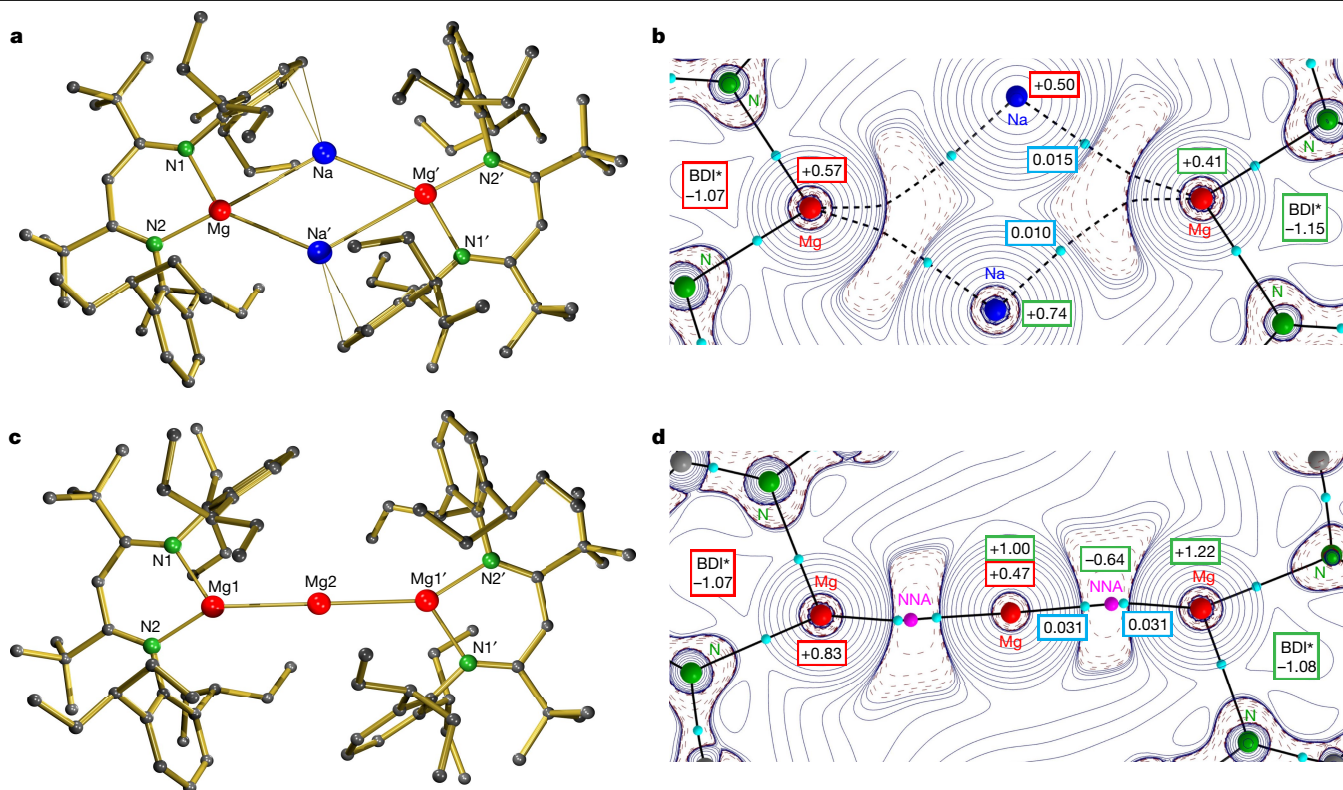


Fig. 3 | Molecular structures and Laplacian distribution of the electron density for the Mg^0 complexes. **a.** Crystal structure of $\{[(\text{BDI}^*)\text{Mg}^0][\text{Na}^+]\}_2$ (**1**). **b.** Laplacian distribution for **1** in the Mg–Na–Mg plane. **c.** Crystal structure of $(\text{BDI}^*)\text{MgMgMg}(\text{BDI}^*)$ (**5**). **d.** Laplacian distribution for **5** in the Mg–Mg–Mg plane. For **b** and **d**: light-blue dots, bond critical point (BCP); purple dots,

non-nuclear attractor (NNA); red boxes, NPA charges; green boxes, AIM charges; light-blue boxes, electron densities in the BCPs. Red dashed lines indicate areas of charge concentration, while blue solid lines show areas of charge depletion.

two bulky monoanionic BDI^* ligands. The unusually high electron density on both Na atoms, combined with a relatively short $\text{Na}\cdots\text{Na}$ distance of 3.1521(8) Å, raises the question of whether there is Na–Na bonding.

Calculations on the diamond-shaped Na_4 cluster, which is isoelectronic to the $\text{Mg}_2\text{Na}_2^{2+}$ core in **1**, predict a short Na–Na bond along one of its diagonals²⁵. Therefore, the electronic structure of Na_4 is completely different, and described by two non-nuclear-attractors (NNA) in the Na_3 units²⁵. These ‘ghost atoms’ are local maxima in the electron density and not officially associated with an atom nucleus. The Laplacian (that is, the second derivative) of the electron density in the MgNa_2 -planes in **1**, however, is in agreement with a lone pair of electrons that is mainly located at the more electronegative Mg but is polarized towards the electropositive Na^+ nuclei (Fig. 3b). AIM and Wiberg analyses do not confirm Na–Na bonding but Mg–Na bonding is supported by bond paths in the AIM analysis as well as by Wiberg bond indices (0.35/0.11 for short/long contacts).

Complex **1** is moderately soluble in benzene and slowly decomposes at room temperature. Addition of ethereal solvents or cryptands, as well as attempts to replace Na^+ by Li^+ or K^+ led to immediate decomposition, indicating the importance of Na^+ cation stabilization²⁶. Solution NMR data are in agreement with high symmetry, implying that the asymmetrically bridged structure found in the solid state is in fast exchange. While dinuclear Mg^{I} complexes are inert to H_2 , a benzene solution of **1** at room temperature turned turbid after H_2 saturation. From the mother liquor, $(\text{BDI}^*)\text{MgH}$ (**2**) was isolated and its crystal structure (Supplementary Fig. 43) reveals a rare three-coordinate Mg hydride complex²⁷, which in C_6D_6 gives a sharp Mg–H ^1H NMR resonance at 3.96 ppm. This reactivity excludes the presence of hidden hydrides in the crystal structure of **1**. The nucleophilicity of the $(\text{BDI}^*)\text{Mg}^-$ anion in **1** was demonstrated by reaction with $(\text{BDI}^*)\text{MgI}$

(**IV**). Comproportionation of Mg^0 and Mg^{II} gave full conversion to $(\text{BDI}^*)\text{MgMg}(\text{BDI}^*)$ (**V**). While reaction of **1** with *n*BuI gave a mixture of $(\text{BDI}^*)\text{Mg}^{\text{I}}n\text{Bu}$ (**VI**) and $(\text{BDI}^*)\text{MgI}$ (**IV**), reaction with PhF (or PhI) led to $(\text{BDI}^*)\text{MgPh}$ (**3**; the crystal structure is given in Supplementary Fig. 44) and NaF (or NaI). Dinuclear Mg^{I} complexes, which generally only activate C(*sp*²)–F bonds in electron-poor aromatics (for example, $\text{C}_6\text{F}_4\text{H}_2$)²⁸, need photolytic activation for such C–F bond cleavage in PhF (ref. 16). Addition of naphthalene to **1** gave $(\text{BDI}^*)\text{MgH}$, indicating C–H activation, but owing to competing decomposition reactions, other unidentified products were also formed.

Dissolved in benzene, complex **1** slowly decomposed at room temperature into two main species, with formation of a metal mirror. Yellow crystals of $(\text{BDI}^*)\text{Na}$ (**4**) could be isolated from the mother liquor (Supplementary Fig. 45). A second crop of crystals was found to contain dark red crystals as well as $(\text{BDI}^*)\text{Na}$. After handpicking and recrystallization, red crystals of $(\text{BDI}^*)\text{MgMgMg}(\text{BDI}^*)$ (**5**) were isolated in a yield of 9%. Elemental analysis of **5** excludes the presence of Na and confirms the Mg_3 core. Accordingly, the metal mirror formed during decomposition was found to consist of Na^0/Mg^0 in a 2/1 ratio, demonstrating that the $(\text{BDI}^*)\text{Mg}^-$ anion in **1** is able to reduce Na^+ . This observation is in line with the unusually low positive NPA charge on Na^+ in **1** (see above). Based on this, we propose two decomposition pathways: (A) $\mathbf{1} \rightarrow 2(\text{BDI}^*)\text{Mg}^* + 2\text{Na}^0$ and (B) $\mathbf{1} \rightarrow 2(\text{BDI}^*)\text{Na} + 2\text{Mg}^0$ (the latter reaction may go through a hypothetical intermediate with interchanged Mg/Na positions, which was calculated to be 21.2 kcal mol^{−1} higher in energy than **1**, see Supplementary Fig. 52). Formation of trinuclear **5** could be envisioned as interception of Mg^0 by two $(\text{BDI}^*)\text{Mg}^*$ radicals.

The crystal structure of **5** is centrosymmetric (Fig. 3c) and the equal Mg–Mg bonds of 2.8876(5) Å are in the range of relaxed Mg^I–Mg^I bonding (compare Fig. 1c). Although Mg and Zn have similar metal and

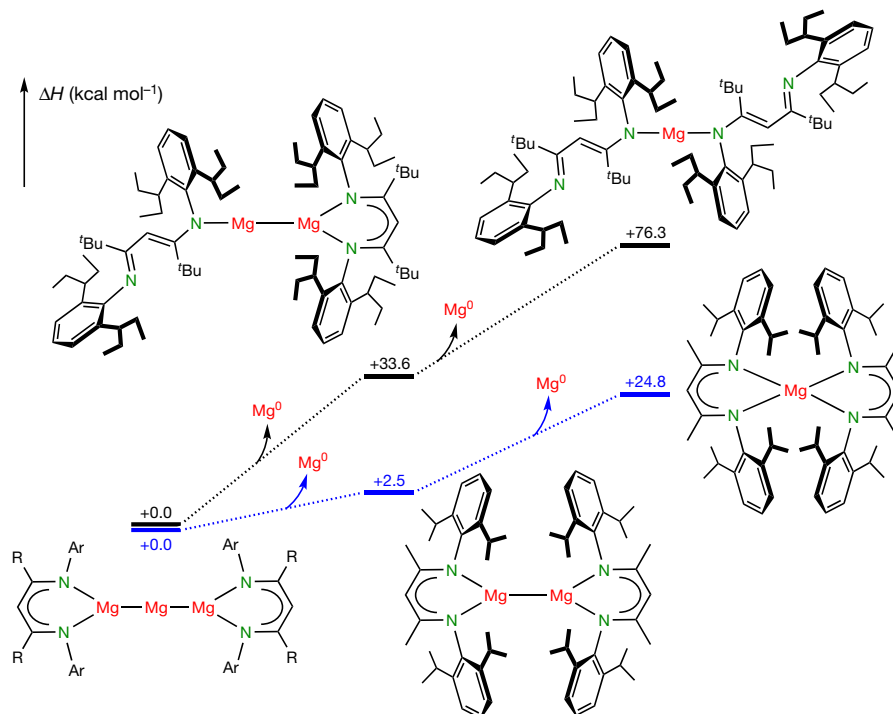


Fig. 4 | Calculated energy profiles for stepwise loss of Mg^0 in trinuclear Mg-Mg-Mg complexes. Energy levels shown black are for stepwise degradation of **5**. Energy levels shown blue are for facile degradation of a

hypothetical complex with a less bulky ligand, highlighting the importance of the ligand bulk for stabilization of **5**.

ionic radii, the Mg–Mg contact is considerably longer than the Zn–Zn bond of 2.384(1)–2.3908(3) Å in related trinuclear Zn–Zn–Zn complexes^{29,30}. The metals in the latter are assigned oxidation states as follows: $\text{Zn}^{\text{I}}-\text{Zn}^0-\text{Zn}^{\text{I}}$. Oxidation state assignment is often ambiguous, but since a negative charge close to unity (–1.07) is calculated for the BDI* ligands in **5**, we propose a similar electron distribution for the $\text{Mg}^{\text{I}}-\text{Mg}^0-\text{Mg}^{\text{I}}$ fragment. The electron-rich character of the central Mg is in line with its low NPA charge of +0.47, while the outer Mg atoms carry charges of +0.88, comparing well to that in Mg^{I} complexes. This electron distribution is supported by average Mg–N bonds of 2.070 Å, typical for chelation of Mg^{I} (see above). AIM analysis gives deviating Mg charges: $\text{Mg}(+1.22)-\text{Mg}(+1.00)-\text{Mg}(+1.22)$ (Fig. 3d). This is due to the presence of two NNAs, each with a basin of 0.64e. Similar NNAs in dinuclear Mg^{I} complexes display a slightly higher electron density of about 0.8e (refs. ^{15,17,31}), see Supplementary Fig. S7. Dividing the electron density of 0.64e in each of these basins equally over the neighbouring Mg atoms, charges of $\text{Mg}(+0.90)-\text{Mg}(+0.36)-\text{Mg}(+0.90)$ result. On the basis of charge analyses, the trinuclear core in **5** is closest to a $\text{Mg}^{\text{I}}-\text{Mg}^0-\text{Mg}^{\text{I}}$ fragment.

NMR data for **5** in C_6D_6 indicate a highly symmetric species. Although the central Mg^0 atom is only bound to two flanking Mg nuclei, complex **5** is surprisingly stable. In C_6D_6 at 80 °C, $(\text{BDI}^*)\text{MgMg}(\text{BDI}^*)$ (**V**) and Mg^0 are formed. At 60 °C, **5** reacts overnight with H_2 , forming $(\text{BDI}^*)\text{MgH}$ (**2**) and Mg^0 . Addition of PhI to **5** led to immediate discoloration of the red solution and formation of $(\text{BDI}^*)\text{MgPh}$ (**3**) and MgI_2 . In reaction with $n\text{BuI}$, an inseparable mixture of $(\text{BDI}^*)\text{MgI}$ (**IV**) and $(\text{BDI}^*)\text{Mg}n\text{Bu}$ (**VI**) was obtained, but the Grignard reagent $n\text{BuMgI}$ was also detected by ^1H NMR spectroscopy. The last reaction already proceeds at –80 °C, demonstrating the high reactivity of the Mg_3 core. This raises the question of whether such trinuclear metal Mg clusters may be fleeting intermediates along the pathway for Grignard formation.

More than a century after its discovery, there is still speculation about the formation of Grignard reagents³². The existence of intermediate mixed-valence Grignard clusters like $\text{Ph}(\text{Mg})_4\text{Cl}$ is supported by MALDI–TOF (matrix-assisted laser desorption/ionization time of flight) mass

spectrometry³³. Results of investigations of Grignard reactions with matrix-isolated ‘atomic’ Mg or small Mg_n clusters also favour the existence of Grignard clusters³⁴. Grignard formation is a classical metal corrosion reaction: electrons leave the metal at cathodic sites and Mg_n^+ clusters enter the solution at anodic sites. Whereas small neutral Mg_n clusters are only held together by weak van der Waals forces³⁵, charged Mg_n^+ clusters are more strongly bound and, up to $n=4$, strictly linear³⁶. A large mixed-valence Mg_{16} cluster was recently identified by mass spectrometry as a component of the product formed by reaction of Cp^*K ($\text{Cp}^* = \text{C}_5\text{Me}_5$) with low-valent MgBr (ref. ³⁷). Trinuclear **5** is the first isolated, fully characterized, mixed-valence Mg cluster. Its linear structure may be representative of proposed cluster Grignard intermediates.

Calculations show that linear multimetalloenes $\text{Cp}(\text{Mg})_n\text{Cp}$ ($\text{Cp} = \text{C}_5\text{H}_5$) with $n > 2$ are unstable towards chain degradation by Mg^0 elimination³⁸. The stability of **5** originates from the superbuly BDI* ligand. DFT calculations on stepwise chain degradation explain how ligand bulk influences the decomposition enthalpies (Fig. 4). The first Mg elimination ($\text{5} \rightarrow \text{V} + \text{Mg}^0$) is endothermic by $\Delta H = +33.6 \text{ kcal mol}^{-1}$. Complex **V** is high in energy due to Mg–N bond cleavage induced by ligand–ligand repulsion. Elimination of a second Mg atom ($\text{V} \rightarrow (\text{BDI}^*)_2\text{Mg} + \text{Mg}^0$) is even more endothermic ($\Delta H = +42.7 \text{ kcal mol}^{-1}$). This is due to the high energy of $(\text{BDI}^*)_2\text{Mg}$, for which the structure of minimal energy was calculated to be a two-coordinate Mg complex with unusual monodentate BDI* ligands. However, if one also considers that further condensation of atomic Mg to $\text{Mg}(\text{s})$ is exothermic ($\Delta H = -35.2 \text{ kcal mol}^{-1}$; ref. ³⁹), decomposition of **5** is essentially thermo-neutral, indicating that the ligand also provides kinetic stabilization. We note that the first Mg^0 elimination from a trinuclear complex with a less sterically demanding BDI ligand is facile (Fig. 4).

With the isolation of Mg^0 complexes that either carry a formal negative charge on Mg or feature a trinuclear Mg–Mg–Mg core, several challenging targets in low-valent Mg chemistry¹⁴ have been met. Their remarkable reactivity predicts that further applications as strong, soluble reducing agents can be expected.

Online content

Any methods, additional references, Nature Research reporting summaries, source data, extended data, supplementary information, acknowledgements, peer review information; details of author contributions and competing interests; and statements of data and code availability are available at <https://doi.org/10.1038/s41586-021-03401-w>.

- Wang, Y. et al. A stable silicon(O) compound with a Si=Si double bond. *Science* **321**, 1069–1071 (2008).
- Sidiropoulos, A., Jones, C., Stasch, A., Klein, S. & Frenking, G. N-Heterocyclic carbene stabilized digermanium(O). *Angew. Chem. Int. Edn* **48**, 9701–9704 (2009).
- Braunschweig, H. et al. Ambient-temperature isolation of a compound with a boron-boron triple bond. *Science* **336**, 1420–1422 (2012).
- Jones, C., Sidiropoulos, A., Holzmann, N., Frenking, G. & Stasch, A. An N-heterocyclic carbene adduct of diatomic tin. :Sn=Sn. *Chem. Commun.* **48**, 9855–9857 (2012).
- Mondal, K. C. et al. A stable singlet biradicaloid siladiborane: (L)₂Si. *Angew. Chem. Int. Edn* **52**, 2963–2967 (2013).
- Li, Y. et al. Acyclic germynes: congeners of allenes with a central germanium atom. *J. Am. Chem. Soc.* **135**, 12422–12428 (2013).
- Glaunsinger, W. S. et al. Structure and molecular motions in alkaline earth hexamines. *Nature* **271**, 414–417 (1978).
- Wu, X. et al. Observation of alkaline earth complexes M(CO)₃ (M = Ca, Sr, or Ba) that mimic transition metals. *Science* **361**, 912–916 (2018).
- Wang, Q. et al. Transition-metal chemistry of alkaline-earth elements: the trisbenzene complexes M(Bz)₃ (M=Sr, Ba). *Angew. Chem. Int. Edn* **58**, 17365–17374 (2019).
- Arrowsmith, M. et al. Neutral zero-valent s-block complexes with strong multiple bonding. *Nat. Chem.* **8**, 890–894 (2016).
- Couchman, S. A., Holzmann, N., Frenking, G., Wilson, D. J. D. & Dutton, J. L. Beryllium chemistry the safe way: a theoretical evaluation of low oxidation state beryllium compounds. *Dalton Trans.* **42**, 11375–11384 (2013).
- Green, S. P., Jones, C. & Stasch, A. Stable magnesium(I) compounds with Mg–Mg bonds. *Science* **318**, 1754–1757 (2007).
- Jones, C. Dimeric magnesium(I) β-diketiminates: a new class of quasi-universal reducing agent. *Nat. Rev. Chem.* **1**, 0059 (2017).
- Jones, C. Open questions in low oxidation state group 2 chemistry. *Commun. Chem.* **3**, 159 (2020).
- Gentner, T. X. et al. Low valent magnesium chemistry with a super bulky β-diketimate ligand. *Angew. Chem. Int. Edn* **58**, 607–611 (2019).
- Jones, D. D. L., Douair, I., Maron, L. & Jones, C. Photochemically activated dimagnesium(I) compounds: reagents for the reduction and selective C–H bond activation of inert arenes. *Angew. Chem. Int. Edn* **60**, 7087–7092 (2021).
- Rösch, B. et al. Mg–Mg bond polarization induced by a superbulky β-diketimate ligand. *Chem. Commun.* **56**, 11402–11405 (2020).
- Hicks, J., Juckel, M., Paparo, A., Dange, D. & Jones, C. Multigram syntheses of magnesium(I) compounds using alkali metal halide supported alkali metals as dispersible reducing agents. *Organometallics* **37**, 4810–4813 (2018).
- Cui, C. et al. Synthesis and structure of a monomeric aluminum(I) compound [HC(CMeNAr)₂]Al (Ar=2,6-*i*-Pr₂C₆H₃): a stable aluminum analogue of a carbene. *Angew. Chem. Int. Edn* **39**, 4274–4276 (2000).
- Hicks, J., Vasko, P., Goicoechea, J. M. & Aldridge, S. Synthesis, structure and reaction chemistry of a nucleophilic aluminyll anion. *Nature* **557**, 92–95 (2018); correction **560**, E24 (2018).
- Dye, J. L., Ceraso, J. M., Lok Tak, M., Barnett, B. L. & Tehan, F. J. Crystalline salt of the sodium anion (Na⁻). *J. Am. Chem. Soc.* **96**, 608–609 (1974).
- Camp, C. & Arnold, J. On the non-innocence of “NacNacs”: ligand-based reactivity in β-diketimate supported coordination compounds. *Dalton Trans.* **45**, 14462–14498 (2016).
- Slater, J. C. Atomic radii in crystals. *J. Chem. Phys.* **41**, 3199–3204 (1964).
- Lambert, C. & von Ragué Schleyer, P. Are polar organometallic compounds “carbanions”? The gegenion effect on structure and energies of alkali-metal compounds. *Angew. Chem. Int. Edn Engl.* **33**, 1129–1140 (1994).
- Cao, W. L., Gatti, C., MacDougall, P. J. & Bader, R. F. W. On the presence of non-nuclear attractors in the charge distributions of Li and Na clusters. *Chem. Phys. Lett.* **141**, 380–385 (1987).
- Gentner, T. X. & Mulvey, R. E. Alkali metal mediation: diversity of applications in main group organometallic chemistry. *Angew. Chem. Int. Edn* **59**, 2–18 (2020).
- Arrowsmith, M. et al. Mononuclear three-coordinate magnesium complexes of a highly sterically encumbered β-diketimate ligand. *Inorg. Chem.* **53**, 10543–10552 (2014).
- Bakewell, C., White, A. J. P. & Crimmin, M. R. Addition of carbon-fluorine bonds to a Mg(I)–Mg(I) bond: an equivalent of Grignard formation in solution. *J. Am. Chem. Soc.* **138**, 12763–12766 (2016).
- Hicks, J., Underhill, E. J., Kefalidis, C. E., Maron, L. & Jones, C. A mixed-valence tri-zinc complex, [LZnZnZnL] (L=bulky amide), bearing a linear chain of two-coordinate zinc atoms. *Angew. Chem. Int. Edn* **54**, 10000–10004 (2015).
- Bakewell, C., Ward, B. J., White, A. J. P. & Crimmin, M. R. A combined experimental and computational study on the reaction of fluoroarenes with Mg–Mg, Mg–Zn, Mg–Al and Al–Zn bonds. *Chem. Sci.* **9**, 2348–2356 (2018).
- Platts, J. A., Overgaard, J., Jones, C., Iversen, B. B. & Stasch, A. First experimental characterization of a non-nuclear attractor in a dimeric magnesium(I) compound. *J. Phys. Chem. A* **115**, 194–200 (2011).
- Garst, G. F. & Ungvary, F. in *Grignard Reagents: New Developments* (ed. Richey, H.) 185–276 (Wiley, 2000).
- Tjurina, L. A. et al. Synthesis of cluster alkyl and aryl Grignard reagents in solution. *Organometallics* **23**, 1349–1351 (2004).
- Imizu, Y. & Klabunde, K. J. Metal cluster vs. atom reactivities: magnesium cluster Grignard reagents. *Inorg. Chem.* **23**, 3602–3605 (1984).
- Köhn, A., Weigend, F. & Ahlrichs, R. Theoretical study on clusters of magnesium. *Phys. Chem. Chem. Phys.* **3**, 711–719 (2001).
- Eriksson, L. A. Accurate density functional theory study of cationic magnesium clusters and Mg⁺–rare gas interactions. *J. Chem. Phys.* **103**, 1050–1056 (1995).
- Kruczyński, T., Henke, F., Neumaier, M., Bowen, K. H. & Schnöckel, H. Many Mg–Mg bonds form the core of the Mg₁₆Cp*₃Br₂K cluster anion: the key to a reassessment of the Grignard reagent (GR) formation process? *Chem. Sci.* **7**, 1543–1547 (2016).
- Velazquez, A., Fernández, I., Frenking, G. & Merino, G. Multimetalloenes. A theoretical study. *Organometallics* **26**, 4731–4736 (2007).
- Chase, M. W. Jr *NIST-JANAF Thermochemical Tables Part 2*, 4th edn (Monograph No. 9, J. Phys. Chem. Ref. Data, American Institution of Physics, 1998).

Publisher's note Springer Nature remains neutral with regard to jurisdictional claims in published maps and institutional affiliations.

© The Author(s), under exclusive licence to Springer Nature Limited 2021

Methods

General considerations

All experiments were conducted in dry glassware under an inert nitrogen atmosphere by applying standard Schlenk techniques or glove-boxes (MBraun). Solvents were degassed with nitrogen, dried over a column with activated aluminium oxide (Innovative Technology, Pure Solv 400-4-MD, Solvent Purification System) and then stored under inert atmosphere over molecular sieves (3 Å). Deuterated solvents were degassed, dried over molecular sieves (3 Å) and stored under an inert atmosphere. NMR spectra were recorded on Bruker Avance III H 400 MHz and Bruker Avance III HD 600 MHz NMR spectrometers. Chemical shifts (δ) are denoted in parts per million (ppm) and coupling constants in hertz (Hz). ^1H and ^{13}C NMR spectra were referenced to the solvent residual signal ($\text{SiMe}_4 = 0$ ppm). Signal multiplicities are described using common abbreviations: s (singlet), d (doublet), t (triplet), quint (quintet) and m (multiplet). Elemental analysis was performed with a Hekatech Eurovector EA3000 analyser and at Kolbe Microanalytical Laboratory (Mülheim/Ruhr).

Starting materials

(BDI*)H (ref. ¹⁷), (BDI*)Mg n Bu (ref. ¹⁷), (BDI*)MgI (ref. ¹⁷), Na/NaCl (ref. ¹⁸) and Na(CH₂SiMe₃) (ref. ⁴⁰) were prepared according to literature procedures. n BuI and halobenzenes were dried over freshly ground CaH₂, distilled and stored over molecular sieves (3 Å) under an inert atmosphere. Phenyllithium (1.9 M in dibutyl ether) was evaporated to dryness, washed with benzene/hexane, dried under high vacuum and subsequently used as solid material. All other reagents were used as received.

Synthetic procedures

[(BDI*)Mg⁻][Na⁺]₂ (1). (BDI*)MgI (1.02 g, 1.33 mmol) and Na/NaCl (2.52 g, 5 wt%, 5.50 mmol) were suspended in benzene (30 ml) and stirred at room temperature for 14 h. The resulting dark brown suspension was filtered and the residue was extracted with benzene (2 × 20 ml). The combined filtrate and extracts were evaporated to dryness and the remaining black coloured solid was washed subsequently with hexane (3 ml) and cold pentane (-20 °C, 2 × 1 ml). [(BDI*)Mg⁻][Na⁺]₂ was obtained as dark brown powder that was dried under a high vacuum (420 mg, 0.318 mmol, 48%). Crystals suitable for X-ray diffraction analysis were obtained by storing a concentrated benzene solution at room temperature overnight.

^1H NMR (600.13 MHz, C₆D₆, 298 K): δ = 1.00–1.03 (m, 48H, CH₃), 1.24 (s, 36H, C(CH₃)₃), 1.69–1.76 (m, 8H, CH₂), 1.80–1.88 (m, 8H, CH₂), 1.92–1.98 (m, 8H, CH₂), 1.99–2.07 (m, 8H, CH₂), 3.04–3.08 (m, 8H, CH), 5.21 (s, 2H, CH-backbone), 6.92–6.96 (m, 4H, CH-arom), 7.00 (d, 7.5 Hz, 8H, CH-arom) ppm. ^{13}C NMR (150.92 MHz, C₆D₆, 298 K): δ = 11.1 (CH₃), 11.7 (CH₃), 24.6 (CH₂), 25.2 (CH₂), 33.4 (C(CH₃)₃), 40.9 (CH), 43.9 (C(CH₃)₃), 95.3 (CH-backbone), 121.3 (C-arom), 125.2 (C-arom), 139.4 (C-arom), 150.8 (C-arom), 172.3 (CN-backbone) ppm. Elemental analysis. Calculated for C₈₆H₁₃₈Mg₂Na₂N₄ ($M = 1,322.67$ g mol⁻¹): C 78.10, H 10.52, N 4.24, Mg 3.68, Na 3.48. Found: C 77.91, H 10.47, N 4.21, Mg 3.63, Na 3.42.

(BDI*)MgH (2). *Method A.* (BDI*)Mg n Bu (110 mg, 0.158 mmol) and phenylsilane (80 μ l, 0.651 mmol) were dissolved in toluene- d_8 (700 μ l) and stirred at 75 °C for 2 d. All volatiles were removed under vacuum and the yellow oily residue was dissolved in pentane (400 μ l), filtered and slowly cooled to -20 °C. At this temperature crystalline blocks suitable for X-ray diffraction analysis deposited after 2 d. Colourless crystals of (BDI*)MgH were isolated by decanting, washed with cold pentane (-20 °C, 1 × 0.5 ml) and dried under vacuum. Yield: 57 mg, 0.089 mmol, 56%.

Method B. [(BDI*)Mg⁻][Na⁺]₂ (96 mg, 0.072 mmol) was suspended in C₆D₆ (700 μ l), degassed and pressurized with H₂ (1.5 bar) in a J. Young NMR tube. The reaction was stirred at room temperature for 2 d and

the resulting pale yellow suspension was evaporated to dryness. The residue was extracted with hexane (1 ml). The extract was concentrated to approximately 200 μ l, filtered and slowly cooled to -20 °C. After 3 d at this temperature, small colourless crystals of (BDI*)MgH were obtained. Crystals were isolated by decanting, washed with cold pentane (-20 °C, 1 × 0.3 ml) and dried under vacuum. Yield: 29 mg (0.045 mmol, 31%).

Method C. (BDI*)MgMgMg(BDI*) (70 mg, 0.054 mmol) was dissolved in C₆D₆ (520 μ l), degassed and pressurized with H₂ (1.5 bar) in a J. Young NMR tube. The reaction was stirred at 60 °C for 2 d, resulting in a metal mirror and a yellow coloured solution. The supernatant was decanted and evaporated to dryness. The resulting yellow oil was dissolved in hexane (200 μ l), filtered and slowly cooled to -20 °C. Leaving it standing at this temperature for 2 d gave small colourless crystals of (BDI*)MgH that were washed with cold pentane (-20 °C, 1 × 0.3 ml) and dried under vacuum. Yield: 22 mg, 0.034 mmol, 32%.

^1H NMR (600.13 MHz, C₆D₆, 298 K): δ = 0.95 (t, $^3J = 7.4$ Hz, 12H, CH₃), 1.00 (t, $^3J = 7.4$ Hz, 12H, CH₃), 1.18 (s, 18H, C(CH₃)₃), 1.70–1.78 (m, 12H, CH₂), 1.80–1.86 (m, 4H, CH₂), 2.99–3.04 (m, 4H, CH), 3.96 (s, 1H, Mg-H), 5.41 (s, 1H, CH-backbone), 6.99 (d, 7.7 Hz, 4H, CH-arom), 7.06–7.09 (m, 2H, CH-arom) ppm. ^{13}C NMR (150.92 MHz, C₆D₆, 298 K): δ = 10.6 (CH₃), 12.3 (CH₃), 25.7 (CH₂), 27.0 (CH₂), 33.0 (C(CH₃)₃), 41.4 (CH), 44.0 (C(CH₃)₃), 96.1 (CH-backbone), 124.0 (C-arom), 125.5 (C-arom), 139.0 (C-arom), 146.4 (C-arom), 177.0 (CN-backbone) ppm. Elemental analysis. Calculated for C₄₃H₇₀MgN₂ ($M = 639.35$ g mol⁻¹): C 80.78, H 11.04, N 4.38. Found: C 80.70, H 11.07, N 4.31.

(BDI*)MgMg(BDI*) (V). A suspension of [(BDI*)Mg⁻][Na⁺]₂ (45 mg, 0.034 mmol) and (BDI*)MgI (52 mg, 0.068 mmol) in C₆D₆ (600 μ l) was stirred at ambient temperature for 2 d. The resulting brownish suspension was evaporated to dryness and extracted with hexane (1 ml). The yellow extract was concentrated to approximately 200 μ l, filtered and slowly cooled to -20 °C. Leaving it standing at this temperature for 4 d gave yellow block-like crystals of (BDI*)MgMg(BDI*). Crystals were isolated by decanting, washed with cold pentane (-20 °C, 1 × 0.2 ml) and dried under vacuum. Yield: 38 mg, 0.030 mmol, 44%. The NMR data match those of (BDI*)MgMg(BDI*) obtained by the original method¹⁷.

(BDI*)MgPh (3). *Method A.* (BDI*)MgI (211 mg, 0.276 mmol) and phenyllithium (24 mg, 0.286 mmol) were suspended in benzene (6 ml) and stirred at room temperature overnight (18 h). All volatiles were pumped off and the residue was extracted with hexane (7 ml). The extract was concentrated to approximately 0.6 ml, filtered and slowly cooled to -20 °C. Overnight, yellow crystals of (BDI*)MgPh suitable for X-ray diffraction analysis deposited. Crystals were isolated by decanting, washed with cold pentane (-20 °C, 2 × 0.5 ml) and dried under vacuum. Yield: 142 mg, 0.199 mmol, 72%.

Method B. [(BDI*)Mg⁻][Na⁺]₂ (60 mg, 0.045 mmol) was suspended in C₆D₆ (600 μ l) and iodobenzene (20 μ l, 0.181 mmol) was added at ambient temperature. The resulting yellow coloured suspension was stirred for 10 min at room temperature and the solvent was removed under vacuum. The residue was extracted with pentane (1 ml), the extract concentrated to approximately 200 μ l, filtered and slowly cooled to -20 °C. Leaving it overnight at this temperature gave yellow crystals of (BDI*)MgPh. Crystals were isolated by decanting, washed with cold pentane (-20 °C, 1 × 0.3 ml) and dried under vacuum. Yield: 34 mg, 0.047 mmol, 53%.

Method C. (BDI*)MgMgMg(BDI*) (40 mg, 0.031 mmol) was dissolved in C₆D₆ (520 μ l) and iodobenzene (15 μ l, 0.135 mmol) was added. The resulting yellow suspension was freed from solvent and the residue extracted with pentane (1 ml). The extract was concentrated to about 200 μ l, filtered and slowly cooled to -20 °C. After 2 d at this temperature, (BDI*)MgPh was obtained in the form of yellow crystals, which were isolated by decanting, washed with cold pentane (-20 °C, 1 × 0.2 ml) and dried under vacuum. Yield: 25 mg, 0.035 mmol, 56%.

Method D. $\{[(\text{BDI}^*)\text{Mg}^-][\text{Na}^+]\}_2$ (63 mg, 0.048 mmol) was suspended in C_6D_6 (600 μl) and fluorobenzene (20 μl , 0.212 mmol) was added. The resulting red coloured suspension was stirred for 10 min at room temperature and all volatiles were removed under vacuum. The residue was extracted with pentane (1 ml), the extract concentrated to approximately 200 μl , filtered and slowly cooled to -20°C . After 2 d, yellow crystals of $(\text{BDI}^*)\text{MgPh}$ deposited, which were isolated by decanting, washed with cold pentane (-20°C , 1×0.3 ml) and dried under vacuum. Yield: 24 mg, 0.034 mmol, 35%.

^1H NMR (600.13 MHz, C_6D_6 , 298 K): δ = 0.79 (t, 3J = 7.4 Hz, 12H, CH_3), 1.00 (t, 3J = 7.4 Hz, 12H, CH_3), 1.24 (s, 18H, $\text{C}(\text{CH}_3)_3$), 1.60–1.68 (m, 4H, CH_2), 1.69–1.86 (m, 12H, CH_2), 3.06–3.12 (m, 4H, CH), 5.44 (s, 1H, CH-backbone), 6.28–6.31 (m, 2H, Mg- C_6H_5), 6.98–7.03 (m, 3H, Mg- C_6H_5), 7.09 (d, 7.7 Hz, 4H, CH-arom), 7.17–7.19 (m, 2H, CH-arom) ppm. ^{13}C NMR (150.92 MHz, C_6D_6 , 298 K): δ = 9.6 (CH_3), 12.2 (CH_3), 24.8 (CH_2), 26.4 (CH_2), 33.0 ($\text{C}(\text{CH}_3)_3$), 41.1 (CH), 44.1 ($\text{C}(\text{CH}_3)_3$), 95.9 (CH-backbone), 123.9 (C-arom), 125.9 (Mg- C_6H_5), 126.1 (C-arom), 126.1 (Mg- C_6H_5), 138.9 (C-arom), 140.9 (Mg- C_6H_5), 146.8 (C-arom), 158.5 (Mg- C_6H_5), 176.7 (CN-backbone) ppm. Elemental analysis. Calculated for $\text{C}_{49}\text{H}_{74}\text{MgN}_2$ (M = 715.45 g mol^{-1}): C 82.26, H 10.43, N 3.92. Found: C 82.27, H 10.63, N 3.88.

(BDI^{*})Na (4). **Method A.** $\text{Na}(\text{CH}_2\text{SiMe}_3)$ (19 mg, 0.172 mmol) and $(\text{BDI}^*)\text{H}$ (106 mg, 0.172 mmol) were suspended in C_6D_6 (600 μl) and stirred at 60°C for 4 h. All volatiles were removed under vacuum and the resulting off-white powder was dissolved in hexane (1.2 ml), filtered and slowly cooled to -20°C . Overnight, pale yellow crystals of $(\text{BDI}^*)\text{Na}$ suitable for X-ray diffraction analysis deposited, which were isolated by decanting, washed with cold pentane (-20°C , 1×0.5 ml) and dried under high vacuum. Yield: 70 mg, 0.110 mmol, 64%.

Method B. $\{[(\text{BDI}^*)\text{Mg}^-][\text{Na}^+]\}_2$ (101 mg, 0.076 mmol) was dissolved in benzene (4 ml) and stirred at 50°C overnight (17 h). The resulting suspension was filtered and evaporated to dryness. The residue was dissolved in hexane (700 μl), filtered and slowly cooled to -20°C . Leaving it standing at this temperature for 4 h gave pale yellow crystals of $(\text{BDI}^*)\text{Na}$ (29 mg, 0.046 mmol, 30%) that were isolated by decanting, washed with cold pentane (-20°C , 2×0.3 ml) and dried under vacuum.

^1H NMR (600.13 MHz, C_6D_6 , 298 K): δ = 0.60 (t, 3J = 7.4 Hz, 12H, CH_3), 1.07 (t, 3J = 7.4 Hz, 12H, CH_3), 1.35 (s, 18H, $\text{C}(\text{CH}_3)_3$), 1.43–1.48 (m, 4H, CH_2), 1.53–1.59 (m, 4H, CH_2), 1.68–1.75 (m, 4H, CH_2), 1.79–1.86 (m, 4H, CH_2), 3.00–3.05 (m, 4H, CH), 5.10 (s, 1H, CH-backbone), 6.88–6.92 (m, 2H, CH-arom), 6.93–6.95 (m, 4H, CH-arom) ppm. ^{13}C NMR (150.92 MHz, C_6D_6 , 298 K): δ = 11.1 (CH_3), 12.7 (CH_3), 26.8 (CH_2), 27.2 (CH_2), 33.1 ($\text{C}(\text{CH}_3)_3$), 40.9 (CH), 44.6 ($\text{C}(\text{CH}_3)_3$), 91.4 (CH-backbone), 119.4 (C-arom), 124.6 (C-arom), 134.3 (C-arom), 153.4 (C-arom), 170.7 (CN-backbone) ppm. Elemental analysis. Calculated for $\text{C}_{43}\text{H}_{69}\text{NaN}_2$ (M = 637.03 g mol^{-1}): C 81.08, H 10.92, N 4.40. Found: C 81.01, H 11.12, N 4.41.

(BDI^{*})MgMgMg(BDI^{*}) (5). $\{[(\text{BDI}^*)\text{Mg}^-][\text{Na}^+]\}_2$ (500 mg, 0.378 mmol) was dissolved in benzene (22 ml) and stirred at 56°C (the yield of complex $(\text{BDI}^*)\text{MgMgMg}(\text{BDI}^*)$ could be optimized by decomposition at 56°C , Supplementary Fig. 7) for 16 h. A defined metal mirror formed on the glass wall. The resulting red-brown suspension was decanted from the metal mirror and evaporated to dryness. The residue was suspended in pentane (3.5 ml), filtered and slowly cooled to -20°C overnight. First a crop of pale yellow crystals of complex $(\text{BDI}^*)\text{Na}$ was obtained. The supernatant was decanted, concentrated (about 2 ml) and stored at -20°C . Leaving it standing overnight gave a mixture of pale yellow crystals of $(\text{BDI}^*)\text{Na}$ and red/brown block-like crystals. The latter were hand selected, dissolved in pentane (600 μl), filtered and slowly cooled to -20°C . After 2 d at this temperature, red-brown block-like crystals of complex $(\text{BDI}^*)\text{MgMgMg}(\text{BDI}^*)$ suitable for X-ray diffraction analysis deposited. The supernatant was decanted and the crystals were washed with cold pentane (-20°C , 2×0.3 ml) and dried under vacuum. Yield: 44 mg, 0.034 mmol, 9%.

^1H NMR (600.13 MHz, C_6D_6 , 298 K): δ = 0.92 (t, 3J = 7.4 Hz, 24H, CH_3), 1.03 (t, 3J = 7.4 Hz, 24H, CH_3), 1.19 (s, 36H, $\text{C}(\text{CH}_3)_3$), 1.71–1.80 (m, 24H, CH_2), 1.80–1.87 (m, 8H, CH_2), 2.90–2.95 (m, 8H, CH), 5.24 (s, 2H, CH-backbone), 7.03 (d, 7.6 Hz, 8H, CH-arom), 7.08–7.11 (m, 4H, CH-arom) ppm. ^{13}C NMR (150.92 MHz, C_6D_6 , 298 K): δ = 11.3 (CH_3), 11.8 (CH_3), 24.8 (CH_2), 26.5 (CH_2), 33.2 ($\text{C}(\text{CH}_3)_3$), 41.3 (CH), 43.7 ($\text{C}(\text{CH}_3)_3$), 95.7 (CH-backbone), 123.1 (C-arom), 125.4 (C-arom), 138.6 (C-arom), 147.7 (C-arom), 174.4 (CN-backbone) ppm. Elemental analysis. Calculated for $\text{C}_{91}\text{H}_{150}\text{Mg}_3\text{N}_4$ (M = 1,373.14 g mol^{-1} , calculated with one co-crystallized molecule of pentane per dimer): C 79.60, H 11.01, N 4.08, Mg 5.31. Found: C 79.21, H 11.09, N 4.01, Mg 5.26. The Na content was found to be 0.02%. This excludes incorrect metal assignment in the crystal structure of 5.

Reactivity studies

Reaction of $\{[(\text{BDI}^*)\text{Mg}^-][\text{Na}^+]\}_2$ with $n\text{BuI}$. $\{[(\text{BDI}^*)\text{Mg}^-][\text{Na}^+]\}_2$ (52 mg, 0.039 mmol) was suspended in C_6D_6 (600 μl) and $n\text{BuI}$ (10 μl , 0.088 mmol) was added in one portion. Immediate discoloration was observed and the reaction mixture was analysed spectroscopically, revealing formation of $(\text{BDI}^*)\text{MgI}$ and $(\text{BDI}^*)\text{MgnBu}$. Repeating the experiment at various temperatures in the range between -80°C and $+25^\circ\text{C}$ did not lead to different reaction outcomes. Crystallization attempts always gave a mixture of crystals of both compounds and therefore separation was not possible.

Reaction of $\{[(\text{BDI}^*)\text{Mg}^-][\text{Na}^+]\}_2$ with naphthalene. $\{[(\text{BDI}^*)\text{Mg}^-][\text{Na}^+]\}_2$ (31 mg, 0.023 mmol) and naphthalene (10 mg, 0.078 mmol) were suspended in C_6D_6 (600 μl) and stirred at room temperature for 3 d. The resulting orange coloured suspension was filtered and analysed by ^1H NMR spectroscopy, which revealed formation of $(\text{BDI}^*)\text{MgH}$ and minor quantities of other unidentified products. Repeating the experiment with deuterated naphthalene- d_8 substantially decelerated the reaction towards the aromatic substrate owing to the kinetic isotopic effect, and formation of $(\text{BDI}^*)\text{Na}$ and $(\text{BDI}^*)\text{MgMgMg}(\text{BDI}^*)$ was observed after 2 d.

Reaction of $(\text{BDI}^*)\text{MgMgMg}(\text{BDI}^*)$ with $n\text{BuI}$. $(\text{BDI}^*)\text{MgMgMg}(\text{BDI}^*)$ (43 mg, 0.033 mmol) was weighed into a J. Young NMR tube and a solution of $n\text{BuI}$ (10 μl , 0.088 mmol) in $\text{THF}-d_6$ (600 μl) was transferred to the tube. This immediately gave a yellow solution, which was analysed by ^1H NMR spectroscopy: signals for $(\text{BDI}^*)\text{MgI}$, $(\text{BDI}^*)\text{MgnBu}$ and the Grignard reagent $n\text{BuMgI}$ were detected. The reaction also proceeds at -80°C , but in that case less formation of $n\text{BuMgI}$ was observed. $n\text{BuMgI}$ rapidly decomposes in solution under formation of 1-butene and precipitation of a colourless powder, and crystallization attempts gave merely crystals of compounds $(\text{BDI}^*)\text{MgI}$ and $(\text{BDI}^*)\text{MgnBu}$.

Analysis of metals formed in decomposition of $\{[(\text{BDI}^*)\text{Mg}^-][\text{Na}^+]\}_2$. $\{[(\text{BDI}^*)\text{Mg}^-][\text{Na}^+]\}_2$ (500 mg, 0.378 mmol) was dissolved in benzene (22 ml) and heated at 56°C for 17 h with gentle stirring. The resulting metal mirror was isolated by decanting, washed with benzene (2×15 ml) and hexane (2×10 ml) and dried under vacuum. After addition of Et_2O (8 ml) to the metal mirror, a HCl solution (2 M in Et_2O , 2 ml) was added via syringe. The resulting colourless suspension was stirred at room temperature for 10 min and evaporated to dryness. The colourless residue was washed with hexane (2×5 ml) and dried under high vacuum at 250°C for 2 h. Yield: 18 mg.

Elemental analysis. Found: Mg 8.39, Na 15.98. This corresponds to a molar ratio of $\text{Mg}^0:\text{Na}^0 = 1:2$. The total equation for the decomposition reaction of complex **1** is therefore: $2\{[(\text{BDI}^*)\text{Mg}^-][\text{Na}^+]\}_2 \rightarrow (\text{BDI}^*)\text{MgMgMg}(\text{BDI}^*) + 2(\text{BDI}^*)\text{Na} + \text{Mg}^0 + 2\text{Na}^0$.

Crystal structure determination

All crystal structures have been measured on a SuperNova (Agilent) diffractometer with dual Cu and Mo microfocus sources and an Atlas

Article

S2 detector. Crystals were embedded in inert perfluoropolyalkylether (viscosity 1,800 cSt; ABCR GmbH) and mounted using a Hampton Research CryoLoop. The crystals were then flash cooled to 100 K in a nitrogen gas stream and kept at this temperature during the experiment. The measured data were processed with the CrysAlisPro (v40.67a) software package⁴¹. Using Olex2⁴², the structures were solved with the ShelXT⁴³ structure solution program using intrinsic phasing and refined with the ShelXL⁴⁴ refinement package using least squares minimization. All non-hydrogen atoms were refined anisotropically. All hydrogen atoms were placed in ideal positions and refined as riding atoms with relative isotropic displacement parameters. The position of hydrides was observed from difference Fourier maps and refined isotropically.

Computational details

All calculations were carried out using Gaussian 16a⁴⁵. All structures were fully optimized without the use of symmetry restraints at a B3PW91/def2svp level of theory^{46–48} including Grimme D3 dispersion correction using Becke-Johnson dampening (GD3BJ)⁴⁹ and checked to be minima by frequency analysis. Energies were determined at a B3PW91/def2tzvp level of theory including Grimme D3 dispersion correction (GD3JB). Charges were calculated at the B3PW91/def2tzvp//def2svp (GD3BJ) level using NBO⁷⁵⁰. The QTAIM analysis was calculated using the B3PW91/def2tzvp//def2svp (GD3BJ) wavefunction with AIMAll 17^{51,52}.

Data availability

X-ray data are available free of charge from the Cambridge Crystallographic Data Centre under references CCDC 2045616 (1), 2045617 (2), 2045618 (3), 2045619 (4) and 2045620 (5). Spectroscopic data that support the findings of this study as well as complementary crystallographic and computational details are included in Supplementary Information. Raw data are available from the corresponding author on reasonable request.

- Clegg, W. et al. Synthesis and structures of [(trimethylsilyl)methyl]sodium and -potassium with bi- and tridentate N-donor ligands. *Eur. J. Inorg. Chem.* 721–726 (2011).
- Rigaku Oxford Diffraction. CrysAlisPro Software system, version 1.171.40.67a (Rigaku Corporation, 2018).
- Dolomanov, O. V., Bourhis, L. J., Gildea, R. J., Howard, J. A. K. & Puschmann, H. OLEX2: a complete structure solution, refinement and analysis program. *J. Appl. Crystallogr.* **42**, 339–341 (2009).
- Sheldrick, G. M. SHELXT — Integrated space-group and crystal-structure determination. *Acta Crystallogr. A* **71**, 3–8 (2015).
- Sheldrick, G. M. Crystal structure refinement with SHELXL. *Acta Crystallogr. C* **71**, 3–8 (2015).
- Frisch, M. J. et al. Gaussian 16 Rev. A.03 (Gaussian, Inc., 2016).
- Becke, A. D. A new mixing of Hartree–Fock and local density-functional theories. *J. Chem. Phys.* **98**, 1372–1377 (1993).
- Perdew, J. P. *Electronic Structure of Solids* (Akademie, 1991).
- Weigend, F. & Ahlrichs, R. Balanced basis sets of split valence, triple zeta valence and quadruple zeta valence quality for H to Rn: Design and assessment of accuracy. *Phys. Chem. Chem. Phys.* **7**, 3297–3305 (2005).
- Grimme, S., Antony, J., Ehrlich, S. & Krieg, H. A consistent and accurate ab initio parametrization of density functional dispersion correction (DFT-D) for the 94 elements H–Pu. *J. Chem. Phys.* **132**, 154104 (2010).
- Reed, A. E., Weinstock, R. B. & Weinhold, F. Natural population analysis. *J. Chem. Phys.* **83**, 735–746 (1985).
- Bader, R. F. W. A quantum theory of molecular structure and its applications. *Chem. Rev.* **91**, 893–928 (1991).
- Keith, T. A. AIMAll Version 17.01.25 (TK Gristmill Software, 2017).

Acknowledgements We thank A. Roth (FAU) and the Kolbe Microanalytical Laboratory (Mülheim/Ruhr) for elemental analysis. This work was generously supported by the University of Erlangen–Nürnberg.

Author contributions B.R.: conceptualization, investigation, validation, formal analysis (that is, analyses of raw data from spectroscopy, X-ray diffraction or computational methods), writing of original draft and visualization. T.X.G.: investigation, validation and formal analysis. J.E.: formal analysis. J.L.: formal analysis. H.E.: formal analysis. S.H.: conceptualization, writing of original draft, review and editing, visualization, supervision and project administration.

Competing interests The authors declare no competing interests.

Additional information

Supplementary information The online version contains supplementary material available at <https://doi.org/10.1038/s41586-021-03401-w>.

Correspondence and requests for materials should be addressed to S.H.

Peer review information *Nature* thanks Jason Dutton and the other, anonymous, reviewer(s) for their contribution to the peer review of this work. Peer reviewer reports are available.

Reprints and permissions information is available at <http://www.nature.com/reprints>.